ACES

DOI: 10.1002/asia.201500401

CHEMISTRY
AN ASIAN JOURNAL
Focus Review

Materials Science

The Role of Intentionally Introduced Defects on Electrode Materials for Alkali-Ion Batteries

Evan Uchaker[a] and Guozhong Cao*[a, b, c]

Abstract: Simple defect modification is a powerful means to improve material intercalation capabilities. It has received considerable interest lately as it can directly alter both the chemical and structural characteristics; techniques of note include cationic disordering, amorphization, doping, partial cation reduction, and manipulation of intrinsic defects. Defects can reduce the stress and the electrostatic repulsion between adjacent oxygen layers, which can directly alter the migration energy and diffusion barriers the alkali ion must overcome during intercalation. Complementary to experimental observations, theoretical predictions are paramount to developing a detailed understanding of material-defect chemistry. This focus review aims to demonstrate that the optimized design of stable intercalation compounds could lead to substantial improvements in energy-storage applications by overcoming intrinsic limitations.

1. Introduction

Energy use plays an increasingly important role in modern society as we move towards increased device portability and diminished fossil fuel consumption. These advancements are spurred by both environmental and economic incentives based on global concern regarding energy efficiency, greenhouse gas emission, and resource scarcity. Global subsidies for fossil fuels totaled $548 billion in 2013 alone, the bulk of which went to oil.[1] This value grossly dwarfs the subsidies for renewable energies, thereby making it difficult for such technologies to gain traction on a purely competitive basis. All this policy exists in spite of the projection that world energy consumption will grow by 56% between now and 2040. Consequently, substantial effort has been made to develop and install renewable energy-harvesting technologies. However, their successful implementation will be dependent on reliable and robust storage devices given that these harvesting methods are intermittent in space and variable in time, and the majority of consumption targets cannot be readily tethered to the grid.[2]

[a] *Dr. E. Uchaker, Prof. G. Cao*
Department of Materials Science & Engineering
University of Washington
302M Roberts Hall, Seattle, WA 98195 (USA)
E-mail: gzcao@u.washington.edu

[b] *Prof. G. Cao*
Beijing Institute of Nanoenergy and Nanosystems
Chinese Academy of Sciences
Beijing 100083 (China)

[c] *Prof. G. Cao*
School of Materials Science and Engineering
Dalian University of Technology
Dalian 116023 (China)

Batteries, as devices for chemically storing energy, possess advantages of high portability, high conversion efficiency, relatively high energy density, long life, and zero exhaust release. They are ideal power sources for portable devices, automobiles, and backup power supplies; accordingly, batteries power nearly all of our portable or mobile electronic devices and are used to improve the efficiency of hybrid electric vehicles as well.[3,4] Unfortunately, considerable improvements in energy density, power density, and stability are still needed to achieve energy sustainability (e.g., smart grid and electric vehicle technologies).[5] Therefore, developing battery technology, particularly rechargeable batteries, has advanced into a crucial issue for academia and industry over the past several years.

Despite years of intensive research accompanied with significant progress, there is significant room for improvement regarding the electrode active materials.[6] The overall capacity and potential cycling window of many electrode materials are limited to prevent degradation over long-term cycling. In addition to exploring new cathode materials there have also been strong efforts to improve the intercalation capacity of already well-established cathode materials. Such developments are incentivized by the fact that approximately 23 and 8% of the overall battery pack costs stem from the cathode and anode active materials alone, respectively.[7]

Electroactive material confinement at the nanoscale has been the primary means through which battery performance has improved over the past decade. Correspondingly, the synthesis and characterization of nanostructured electrode materials of various chemistries have been extensively investigated. Nanomaterials themselves possess high surface energy and can therefore be considered as deviated from their equilibrium state.[8] However, nanomaterials as a whole suffer from several basic limitations that restrict their performance in energy-storage applications;[9,10] additionally, as a result of their small size

and obtrusive surface effects, the introduction of defects can play a tremendous role in property (and subsequent performance) alteration. Thus, it is necessary to utilize either one or several exploitive techniques that can easily increase battery performance for renewable-energy resources to achieve cost parity with traditional energy sources. Herein, this focus review strives to shed light on the positive effects that the intentional introduction of defects can have on the performance of electrochemically active materials for alkali-ion battery electrodes. Lithium- and sodium-ion battery systems will be briefly introduced, as will some of the more common defects researchers can readily control and employ. Findings from the literature will then be reviewed; ultimately, the role of defects in transition-metal-based electrode active materials and their corresponding electrochemical properties will be highlighted.

2. Alkali-Ion Battery Electrode Chemistry

An alkali-ion battery consists of several electrochemical cells connected in parallel and/or in series to provide a designated capacity or voltage. Each electrochemical cell has two electrodes separated by an electrolyte that is electrically insulating but ionically conductive. During discharge, when the alkali-ion battery operates as a galvanic cell, alkali ions exit the negative electrode (typically carbon) and insert themselves into the positive electrode (typically some layered transition-metal oxide (TMO) compound), while electrons move externally from the negative electrode to the positive electrode. During charge, or when it operates as an electrolytic cell, the process is reversed by means of an externally applied electromotive (potential-based) force. The total energy stored in and released by a cell during charge and discharge is controlled by the thermodynamics and kinetics processes of the active electrode material.

Among the many types of rechargeable batteries, Li-ion batteries (LIBs) are a mature and robust technology that have been extensively used in consumer devices and industrial applications, and are heralded for their high energy and power densities.[11] Compared to the comprehensive body of work on lithium-ion batteries, research on sodium-ion batteries (NIBs) is still in its nascent stages.[12] A Na-ion battery functions under the same principles as Li-ion technology, but with different characteristics as dictated by the properties of the transporting ionic species and the consequent effects this has on the electrode materials (Table 1).[13] Sodium and lithium have similar chemical properties including ionicity, electronegativity, and electrochemical reactivity as they are both alkali metals. However, the larger size and different bonding characteristics of sodium ions influence the thermodynamic and/or kinetic properties of sodium-ion batteries, and can lead to unexpected behavior in terms of electrochemical performance or reaction mechanism.

For a given electrode material, the composition, crystal structure, and morphology can dictate the reaction rate and transfer processes, and can be manipulated to alter the overall electrochemical performance. There are several ways in which alkali ions can be repeatedly incorporated and removed from the electrode electroactive material. The three main mechanisms through which lithiation or sodiation occur are based on intercalation, alloying, and conversion reactions.

Table 1. Comparative qualities of lithium and sodium for alkali-ion battery application.

Parameter	Lithium	Sodium
cationic radius [Å]	0.76	1.06
atomic weight [g mol^{-1}]	6.9	23.0
E° (V vs. SHE)	−3.04	−2.71
carbonate cost [$/ton]	6000	150
metallic capacity [mA h g^{-1}]	3829 (Li^+)	1165 (Na^+)
metallic capacity [mA h cm^{-3}]	2062 (Li^+)	1131 (Na^+)
coordination preference	octahedral and tetrahedral	octahedral and prismatic

Of the three methods, intercalation is by far the most thoroughly investigated and well understood, and was the system on which initial developments in LIBs were based. Intercalation is the reversible insertion of a guest species (ion or molecule) into the lattice of a lamellar host structure. It can also occur in three-dimensional crystals with available empty oxygen tetrahedra and octahedra. The overall process of electrochemical intercalation can be broken down into three simultaneous and sequential processes: 1) redox reactions at the electrode–electrolyte interface, 2) nucleation and growth of the new interfacial phase, and 3) charge and mass transfer. The structure of the host remains unchanged or is only slightly altered in the guest–host complex with the inclusion of the intercalation

Guozhong Cao is the Boeing-Steiner Professor of Materials Science and Engineering, Professor of Chemical Engineering, and Adjunct Professor of Mechanical Engineering at University of Washington, and also a Professor at Beijing Institute of Nanoenergy and Nanosystems, Chinese Academy of Sciences and Dalian University of Technology. His current research is focused on chemical processing of nanomaterials for energy-related applications including solar cells, rechargeable batteries, supercapacitors, and hydrogen storage.

Evan Uchaker received his PhD in Materials Science and Engineering at the University of Washington under the supervision of Professor Guozhong Cao. His research interests are focused on the development and understanding of kinetically stabilized and defected electrode materials for electrochemical energy-storage devices; this mainly encompasses alkali-ion batteries, but also power electronics.

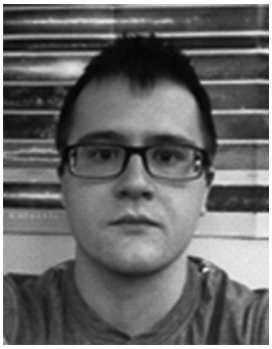

compound (intercalate); however, there can be phase changes depending on the degree or extent of intercalation. The rate of intercalation can be controlled by imposing an external potential across the cell, and the reaction will stop when this potential equals the free energy of the system. Deintercalation will occur when the voltage exceeds this free energy.

The following considerations will be made as related to intercalation-based system chemistries alone, mostly because their synthesis and characterization is more straightforward and the corresponding results are therefore easier to interpret.

2.1. Transition-Metal Oxide Electrodes

Many of the TMO host materials share crystallographic traits, typically with a simple layered, spinel, or olivine-derived structure, however, they often reveal tremendously varying electrochemical properties owing to the unique electronic structure of each TM. Variations in alkali-ion concentration alter the electronic properties of the TMO host material as the alkali-ion valence electron is donated, thereby shifting the valence state or modifying the TM–O bonding characteristics. The valence electronic structure formed between the TM and oxygen ions that comprise the host material is incredibly flexible, and can lead to quite large alkali-ion concentrations within these materials. These valence electrons play a key role in determining the electronic properties of the TMO, and are largely made of TM d-orbital and oxygen-ion p-orbital interactions. Experimentally, it has been demonstrated that the energy conversion accompanying alkali-ion intercalation can be attributed to the electron redox energy and the Madelung potential at the alkali-ion sites as related to the electron and alkali-ion intercalation, respectively.[14,15] For intercalation compounds, the redox reaction depends on the formal valence-state alternation of the active cation and its covalent bonding with the nearest-neighbor anions.[11]

The TM is octahedrally coordinated by oxygen in both the layered and spinel crystal structures. Within this coordination, the degeneracy, which would exist in the free TM ion, of the d-orbitals is broken as viewed through crystal-field theory. Molecular orbital theory expands upon this in that the TM d-orbital and oxygen-ion p-orbital directly overlap yielding bonding and antibonding σ levels. It follows that other levels arise from the overlap between the TM 4s and 4p orbitals with the oxygen-ion p-orbitals. All this is complicated by the fact that the octahedral site typically adopts an imperfect geometry, disrupting the degeneracy even further. Alkali-ion removal can lead to structural destabilization or order–disorder phase transitions.

A schematic of the relevant energy levels in the electrodes and the electrolyte of a thermodynamically stable LIB relative to one another is shown in Figure 1. The energy separation (E_g) between the lowest unoccupied molecular orbital (LUMO) and the highest occupied molecular orbital (HOMO) of the electrolyte represents the potential window over which the electrolyte can reversibly function. The two electrodes serve as electronic conductors with anode (reductant) and cathode (oxidant) electrochemical potentials of μ_A and μ_C, respectively. If the employed anode has a μ_A value above the electrolyte

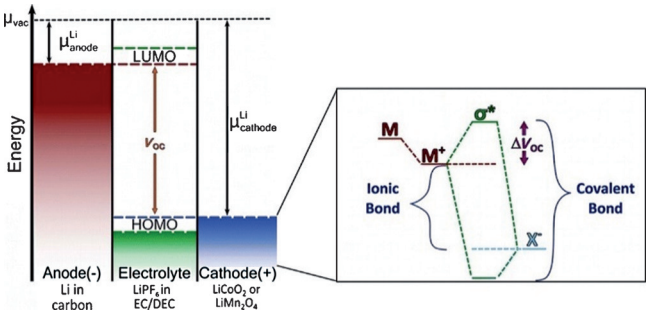

Figure 1. Schematic illustration of the energy levels involved in a typical Li-ion electrochemical cell. The dashed red, blue, and green lines correspond to the Fermi energy of Li in the anode, the lowest energy level of the transition-metal antibonding states, and a typical placement for the voltage window for the electrolyte, respectively. V_{OC} is the open circuit potential of the cell, and μ is the chemical potential. The difference between the energy associated with the stabilization in the two extremes sets the boundary for the maximum amount of tuning of the V_{OC} that can be obtained through structural modification. Reprinted with permission from Melot et al., *Acc. Chem. Res.* **2013**, *5*, 1226–1238. Copyright 2013 American Chemical Society.[16]

LUMO, then the electrolyte will be reduced unless the anode–electrolyte reaction becomes blocked by the formation of a passivating layer (solid electrolyte interphase, SEI). The same occurs for a cathode with a μ_C value below the HOMO, but μ_C cannot be lowered below the top of the cathodic anion p bands, which may have an energy above the electrolyte HOMO; thus, the voltage of many layered oxides is intrinsically self-limited by the top energy of the O 2p bands. Therefore, the electrode electrochemical potentials μ_A and μ_C must reside within the electrolyte window to ensure thermodynamic stability, thereby constraining the open-circuit voltage of the battery cell.

3. Defect Chemistry

Defects play an important part in both the chemical and physical behavior of solids. Often the term "defect" has connotations of some negative side effect. However, much of modern science and technology centers upon the exploitation or suppression of the properties that defects confer upon a solid. In this sense, defects are a tool to be utilized at one's disposal. Some of the more common defects include point, line, and plane defects in the form of vacancies; interstitial, dislocation, and stacking faults; and grain boundaries.

Simple defect modification is a powerful means to improve material intercalation capabilities. It has received considerable interest lately as it can directly alter both the chemical and structural characteristics; techniques of note include cationic disordering, amorphization, doping, partial cation reduction, and manipulation of intrinsic defects (i.e., oxygen vacancies, denoted $V_O^{\bullet\bullet}$ in Kröger–Vink notation).[17–25]

Defects can directly impact alkali-ion intercalation by shifting the thermodynamics and improving the kinetics.[26] The presence of defects increases the system energy and they can potentially serve as nucleation sites that facilitate the electrochemical phase transition. Surface-reaction-limited (SRL) dy-

namics predict that the phase boundary extends from surface to surface along planes of fast ionic diffusion in which defects or facet edges can act as nucleation sites.[27] Such results have been verified experimentally, where defects have been reported to promote the phase transition by providing low-energy mass-transport routes during the phase-transition process.[28,29] Defects may also reduce the stress and electrostatic repulsion between adjacent oxygen layers, which can directly alter the migration energy and diffusion barriers the alkali ion must overcome during intercalation.[30]

The resulting performance impact of defect introduction is not always as straight forward as would be expected. For example, the addition of defects can modify the covalency of the electroactive species or the long-range interaction between alkali ions of different crystallographic planes. Experimentally, it has been observed that it is possible to suppress the cathode-electron energy level by increasing the ionic nature of the electrode material. The position of the cathodic conduction-band states can be directly determined by metal–ligand (MX) bonding characteristics and is reflected in the interatomic distances, in which short distances imply stronger (predominately covalent) bonds. Increasing the ionic contribution to the bonding coincides with a decrease in the separation between the bonding (σ) and antibonding (σ^*) orbitals (or any splitting of degenerate orbital states, which are often seen in transition-metal oxides); this in turn gives rise to a greater difference in energy between the alkali-ion 1s and the lowest-unoccupied 3d metal levels (σ^*). This ultimately increases the cell potential, and has come to be known as the inductive effect (Figure 1); it has been demonstrated experimentally as a way to tune redox potentials in a wide variety of systems. Through this mechanism, it is possible to adjust the open-circuit voltage through structural modification, which in turn alters the charge density of the MX bonds.[16] The following is a summation of the most common and impactful defects in alkali-ion battery electrode materials.

3.1. Disordering

Cation disorder involves the intermixing between the alkali-ion and the transition-metal sublattice, and is more likely to exist in systems in which there are varying redox sites, be it in the form of several transition-metal elements or a single multivalent element. Disordering has been shown to increase the solid-solution behavior, reduce the two-phase transformation domains, lower the alkali-ion extraction energy, and modify the diffusion/transport properties during the de/intercalation processes.[17,31–36] The volumetric expansion and changes in lattice parameters, as a function of inserted alkali-ion concentration, are seemingly negligible in disordered materials (typically on the order of $<1\%$). This in turn leads to less mechanical stress and superior capacity retention for an electrode material; minimal structural change is also conducive to substantially enhanced alkali-ion mobility. Additionally, disordered materials tend to experience less change in their local alkali-ion environment, as a function of state of charge, because of a more homogeneous cation distribution.

3.2. Amorphization

Interest in amorphous material hosts has been steadily growing over the past several years. Crystalline hosts are formed at elevated temperatures, which means that particle growth is often inevitable, whereas amorphous electrodes can be prepared at low or even ambient temperatures thereby preserving the active state of the constituents and suppressing particle growth. Furthermore, this saves time and energy during production.

From an operation standpoint, the storage capacity in crystalline materials is critically dependent on several factors including guest-ion site energy, crystal-growth orientation, exposure of electrochemically active facets, as well as phase transitions and structural stability.[37] By contrast, the use of amorphous structures is proposed to work in a similar manner to disordering in that it can ease the diffusion of incoming ions by providing a more open framework for ion migration.[18,38–41] Amorphous electrodes often demonstrate improved kinetics because there is no macroscopic phase transition. The greater Gibbs free energy of formation of kinetically stable amorphous phases enhances the cell potential and potential window over which the material can reliably operate, thus boosting the cell energy density.[42,43]

3.3. Doping

Doping is often used as a means to achieve partial cation reduction—although the latter can be successfully done without such means—to introduce mixed-valence states into the transition metal and, thus, tune the electronic transport properties of the material.[44] Mixed conductivity is necessary, both electronically and ionically, at the atomic scale for charge-neutrality preservation during alkali-ion transport, at which the chemical diffusion coefficient is ultimately rate-limited by the slower of the two processes. The introduction of oxygen vacancies is well known to increase the conductivity in oxide materials.[45,46] Supervalent metal doping has demonstrated its ability to significantly increase the electronic conductivity, effectively overcoming the low intrinsic limitations of several materials.[47]

3.4. Nonstoichiometry

Although doping of foreign elements (solid-solution-limited dissolution) into some host compound is the most common approach used to improve phase properties, there are several alternative strategies that can also be exploited. One such method involves the introduction of native defects (i.e., oxygen nonstoichiometry).

Several studies have been devoted to examining the effects of lithium nonstoichiometry in LIB electrodes, particularly for $LiCoO_2$, in which such effects are accommodated by oxygen vacancies that can also be accompanied by either cation mixing and/or a perturbation of the oxygen stacking layers. Accordingly, the local environment of some cobalt ions can be modified by the presence of the oxygen vacancies. The structure of these lithium overstoichiometric compounds makes

them more stable against the (de)lithiation process and is a beneficial approach towards preventing structural distortion, and thus shows potential for LIB electrode development.[48,49] Notwithstanding, the recent rejuvenation in NIB research activity has revealed, if not anything else, that analogous materials can behave substantially different than expected based on their prior LIB performance.[50] There have been a minimal number of reports concerning the role of defects in NIB electrode materials and the potential impact they may have on the overall electrochemical performance.[51,52]

3.5. Surface defects

Surface defects present at the electrode–electrolyte interface are expected to serve as nucleation sites that promote phase transitions between the redox and charge/mass transfer processes. As nucleation sites, surface defects may lead to the propagation of the transitioning phases into the bulk of the electrode upon cycling or potentially enhance the charge transfer. Surface defects have been documented as having the ability to dominate the electrochemical properties.[53]

Electrode materials displaying surface defects have been commonly synthesized by annealing the pristine materials with a reactive gas or through substitutional doping techniques. The difficulty introduced with such techniques is that of maintaining the desired local chemistry while controlling the physical features at the same time. Suitable manipulation of the surface chemistry and introduced defects may also serve as a buffer zone to protect the electrode material from the electrolyte when submitted to prolonged cycling, or in such cases where the charging process is discontinuous (i.e., frequency regulation); however, the principle aims of employing surface defects are to enhance the Li^+ storage capacity and improve the overall electrode kinetics.

4. Graphene and Carbon

In studies less focused on defect formation and characterization, Guo et al. synthesized carbon–carbon nanotube composites by means of a soft-templated self-assembly process.[54] The porous and defect-rich structure was initially frozen into the sample by carbonization, but both effects were lost due to solid-state amorphization upon cycling. This loss was accompanied by a steep drop in the capacity after the initial cycle and noticeable capacity fading upon cycling. Reddy et al. demonstrated that the Li^+ capacity and cycle stability were greater in nitrogen-doped graphene than in undoped graphene, and ascribed the discrepancy to the introduction of surface defects into the system.[55] Disordered graphene nanosheets have also been shown to enrich Li^+ capacity owing to additional reversible storage sites such as edges and other defects.[56]

DFT results have also suggested that the presence of grain boundaries in graphene will enhance the Li adsorption significantly, as displayed in Figure 2. Moreover, the energy barrier for the diffusion of a Li adatom along the gain boundary is smaller than that normal to the boundary, which suggests that grain boundaries may channel Li^+ ions during the lithiation

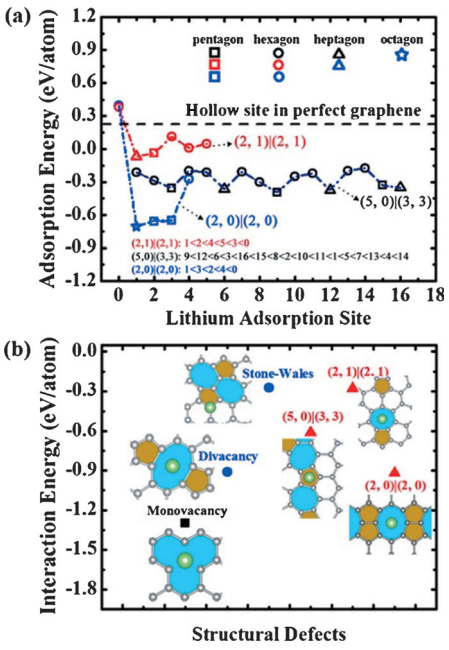

Figure 2. a) The adsorption energy of a Li adatom on different sites in the boundaries. b) Interaction energy of a Li adatom with different structural defects such as a monovacancy, divacancy, Stone–Wales defect, and grain boundaries of several orientations. Insets are the local atomic structures for the most stable adsorption sites of a Li adatom on these five structural defects. Reprinted with permission from Zhou et al., *J. Phys. Chem. C* **2014**, *48*, 1226–1238. Copyright 2014 American Chemical Society.[57]

process. Thus, not only can point, edge, and dopant defects enhance the lithium adsorption of graphene, so can grain boundaries.[57]

Graphite is the most commonly used anode material for LIBs, but its application in NIBs is severely limited. This was corroborated recently by theoretical calculations showing that the minimum interlayer distance necessary for Na^+ ion insertion is 0.37 nm (the interlayer distance of graphite $\approx$0.34 nm).[58] Recently, many carbon nanostructures and derivatives have been found to be receptive to Na^+ insertion, but they rely on the presence of graphite nanocrystallites and nanovoids, which is less than ideal seeing as the latter only takes place over a low and narrow potential range.[59]

First-principles calculations regarding Na adsorption on graphene with various percentages of divacancies (the most common type of vacancy defect observed) and Stone–Wales defects show that adsorption is not possible for pristine graphene. However, the presence of defects enhances the adsorption, and the potential is larger when the adatoms are on and/or around the defective zone. With the increase in defect density, the maximum capacity obtained is much higher than that of graphite and it increases with the density of the defects. For the Stone–Wales maximum possible highest-density divacancy defects, capacities of 1070 and 1450 mA h g^{-1}, respectively, can be achieved. The divergence in performance from pristine graphene is due to changes in the bonding charge distribution leading to enhanced charge transfer. Similar findings were observed for Li and Ca adsorption,[51,60] and such findings have been experimentally verified in half-cells by other groups.[61]

For a porous graphene network, it was shown that divacancy defects can act as seed points that initiate plating of lithium metal within the interior of the porous network structure.[62] This is preferential in that it controls metallic lithium formation and circumvents dendritic growth, which can be unpredictable and pose a safety concern. This entrapment of lithium metal results in very high specific capacities and energy densities of approximately 850 mA h g^{-1} and 547 W h kg^{-1}, respectively. As expected, based on the proposed plating process, the charge-storage capacity increased with the relative level of defectiveness. Unlike graphitic carbon, there is no voltage plateau below 250 mV, but rather a gradual slope below 1 V, which indicates that a different reaction mechanism is at play. X-ray diffraction (XRD) and X-ray photoelectron spectroscopy (XPS) analyses lead to the conclusion that the primary reaction mechanism is lithium-metal plating, in which Li_3C_8 catalyzes an increase in the localized charge density that initiates plating.

Expanded graphite was produced by initially forming graphite oxide that was then partially reduced to limit the large amount of oxygen-containing groups that sterically hinder the sodiation process. When tested, the expanded graphite delivered a high reversible capacity of 284 mA h g^{-1} at a current density of 20 mA g^{-1}, with superior capacity retention (73.92% after 2000 cycles at 100 mA g^{-1}).[63] The defects enhance sodiation because of the strong ionic binding energy between the Na^+ ions and the defects, which effectively overcomes the van der Waals interaction between the graphene sheets. Moreover, larger interlayer distances and defects may account for both the sloped and flat regions observed in the potential profiles of disordered carbon atoms.[64]

5. Transition-Metal Oxides and Derivatives

There are a host of transition-metal-based systems for which the role of defects have been examined. Complementary to experimental observations, theoretical predictions are paramount towards developing a detailed understanding of material-defect chemistry.[52,65–67] However, only a handful will be covered in the following section for the purpose of remaining succinct.

5.1. Titanium Oxide

Titanium dioxide is capable of tolerating fairly high oxygen deficiencies ($TiO_{2-\delta}$) that can be formed either through the removal of oxygen from the anion sublattice, leaving oxygen vacancies, or by the infusion of titanium interstitials. However, Magnéli phases will form at considerably high deviation from the ideal stoichiometry.[68] There are several ionized oxygen vacancies that need be considered for a given temperature range, most notably fully ionized vacancies ($V_O^{\bullet\bullet}$), but also singly ionized ($V_O^{\bullet}$) or even neutral (V_O^{x}) vacancies.

Shin et al. recently studied the role and concentration dependency of oxygen defects in TiO_2 through thermal treatment involving hydrogen reduction (Figure 3).[69] Pristine TiO_2 was compared with argon and hydrogen-treated nanoparticles, where the treatment time varied between one and seven hours. The electronic conductivities follow the Arrhenius form with activation energies determined during heating and cooling. The activation enthalpies for the pristine and hydrogen-treated samples were nearly identical, which indicate that the mechanism of conduction does not change during reduction and that the nonstoichiometry is locked into the material. The conductivity actually increased by one and then two orders of magnitude after hydrogen thermal treatment for one and seven hours, respectively.

The electronic conductivity is limited to the bulk value of anatase. Compared to Ar-annealing, H_2 thermal treatment effectively increases the bulk value of the electronic conductivity and thus not only gives enhances the capacity at low C rates but also improves storage kinetics at high C rates. Based on impedance analysis, the lithium-ion diffusivity for the one-hour

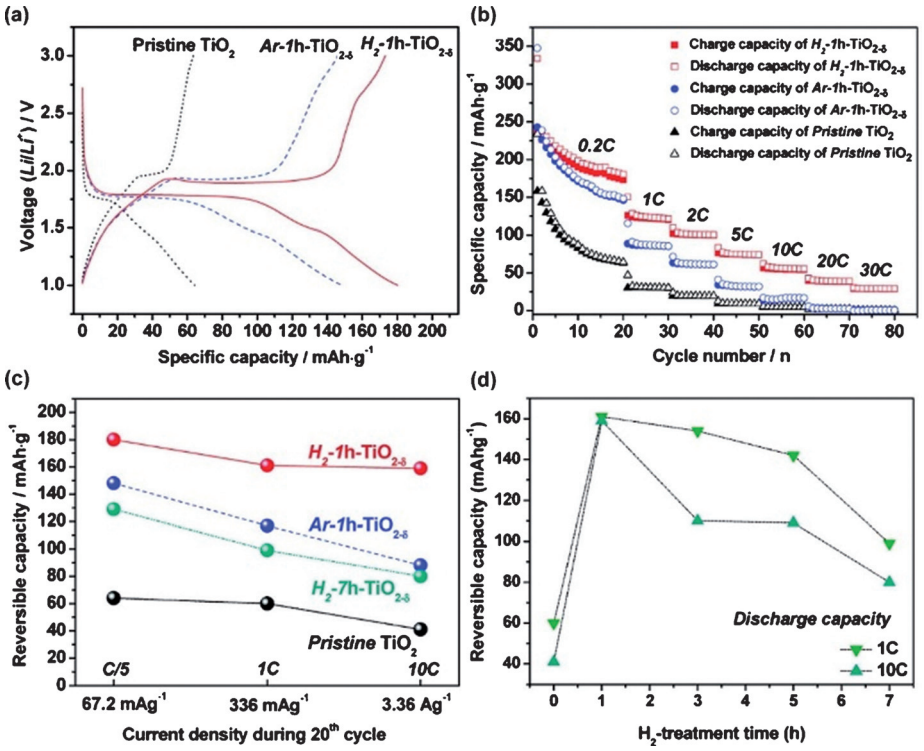

Figure 3. a) Galvanostatic dis/charge profiles (20th cycle) for pristine and various thermally treated $TiO_{2-\delta}$ cycled at 0.2 C. Comparison of the b) rate performance (open: discharge; filled point: charge) and c) current density dependence (20th cycle). d) Reversible capacities of hydrogen-reduced titania during discharge processes at 1 and 10 C as a function of hydrogen-treatment time. Reprinted with permission from Shin et al., *Chem. Mater.* **2012**, *3*, 543–551. Copyright 2012 American Chemical Society.[69]

hydrogen thermal treatment was an order of magnitude higher than that of stoichiometric TiO_2, whereas the material treated for seven hours was roughly equivalent. These results were corroborated by cyclic voltammetry (CV) analysis applying the Randles–Sevcik equation. As expected, the H_2 thermally treated material was effective towards enhancing electrochemical performance, as was the Ar-annealed material. More explicitly, the argon and hydrogen specimens treated for one hour measured capacities of 148 and 180 $mA\,h\,g^{-1}$, respectively, whereas pristine TiO_2 only achieved 64 $mA\,h\,g^{-1}$. This enhancement can be attributed to a denser electrode morphology with better crystallinity, particularly at particle surfaces. However, too high a degree of reduction can be detrimental to performance.

Based off the physical property and electrochemical analysis, a defect model was proposed for $TiO_{2-\delta}$.[70] It was revealed that too high a degree of reduction can actually have deleterious effects caused by a drop in the free Li^+ concentration owing to association with excess electrons. Thus, the electronic concentration is compensated by oxygen vacancies, whereas Li^+ defects dominate at low δ levels. Thus, this model effectively explains how greater H_2 treatment can lead to greater electronic but diminished ionic conductivity.

The same general trend was observed for TiO_2 nanotube arrays annealed in CO and N_2; the improved intercalation capacity and rate capability of the CO-annealed arrays was attributed to the presence of surface defects and cation groups with oxygen vacancies, which not only improved the charge-transfer conductivity of the arrays but also promoted the phase transitions.[71] These results very clearly show the need to optimize defect concentration, and the significance balancing both the electronic and ionic transport can have on achieving high-rate-capability electrode materials.

The use of amorphous TiO_2 has also proven beneficial for Li-ion battery application over its crystalline counterpart both in terms of capacity and rate capability.[20,72,73] EIS examination revealed that crystalline TiO_2 is more electronically conductive than its amorphous counterpart, most likely due to the lack of long-range structure and a higher presence of defects that can act as scattering sites for electron transport. However, EIS also indicated that amorphous TiO_2 has a considerably higher Li^+ diffusivity than its crystalline analogue, most likely because of expansion of the interlayer that lithium occupies. This increased number of defects and expanded interlayer distance also leads to an extended potential range and removal of plateaus in the dis/charge profiles.[38]

These findings were further demonstrated in the Na-ion battery system by Xiong et al. who found that the capacity of amorphous titanium dioxide nanotube electrodes improves with cycling, eventually reaching a maximum of 150 $mA\,h\,g^{-1}$.[41] CV and power-law relationships were utilized to determine the storage process(es) at play. It was found that the discharge process starts as a mainly capacitive-limited mechanism that converts to a mixed contribution (diffusion and surface capacitance) as the potential drops below a certain threshold. Observation of the pre-edge X-ray absorption near-edge structure (XANES) feature suggested an increase in the structural disorder upon Na^+ intercalation, but this eventually reached a saturation point that coincided with the maximum capacity attainable. It was further speculated that the capacity becomes limited as some of the intercalation sites remain inaccessible and some of the Na ions irreversibly remain in the structure. These results highlight some of the potential, and often unexpected, differences that can arise from the use of amorphous electrode materials.

5.2. Vanadium Oxide

Liu et al. investigated the effects of surface defects on the electrochemical performance by annealing V_2O_5 aerogels in different reactive environments (N_2 and air).[20,74] The N_2-annealed films adopted a less crystalline structure composed of particles with smaller grain size. The N_2-annealed films also had a narrower bandgap than the air-annealed films, and the color indicated that the vanadium valence state was a mix of V^{3+} and V^{4+}. Both of these effects could be attributed to the existence of defects in lower valence states. Electrochemical impedance spectroscopy confirmed an improved electrical conductivity in the N_2-annealed V_2O_5 films with defects such as V^{4+}, V^{3+}, and oxygen vacancies. The N_2-annealed films also showed considerably enhanced capacity and cycle stability when compared to the air-annealed films. The discrepancy between the two films was also attributed to the presence of surface defects, which can act as nucleation centers in the phase transition during Li^+ de/intercalation. Another group also confirmed this finding by comparing the Li^+ capacity of pristine and O_2/H_2O-treated V_2O_5, and attributed the difference in the electrochemistry of the two materials to the nonstoichiometric and surface point defects, which serve as additional charge-storage sites.[75]

Sun et al. also explored the role of defects on electrochemical performance by synthesizing highly ordered and defect-rich vanadium oxide nanorolls, further corroborating the importance of defects in improving the electrode material performance.[76] The defected VO nanorolls exhibited superior capacity and cycle stability compared to the pristine VO nanorolls, results that were related to the V^{4+}/V^{5+} ratio, detectable cracks in the wall surfaces, and residual organic surfactant. The electrochemical enhancement was attributed to the additional redox sites that result from the atomic-scale disorder and the enhanced accessibility of Li^+ to the nanorolls because of cracks in between the layers and present due to defects. The results suggest that perfectly ordered materials may not be the ideal structure for electrochemical applications due to the limited ion-diffusion rate.[76]

Tepavcevic et al. electrochemically synthesized nanostructured bilayered vanadium pentoxide, the structure of which was confirmed by synchrotron-based XRD and X-ray absorption spectroscopy (XAS) as well as TEM (Figure 4).[77] Intercalated water residing within the interlayer spacing was removed through a simple vacuum annealing step, and its electrochemical performance was compared with orthorhombic V_2O_5 synthesized by means of a more traditional approach. The structure is composed of stacked V_2O_5 bilayers made of base-oriented square-pyramidal VO_5 units that are arranged parallel to

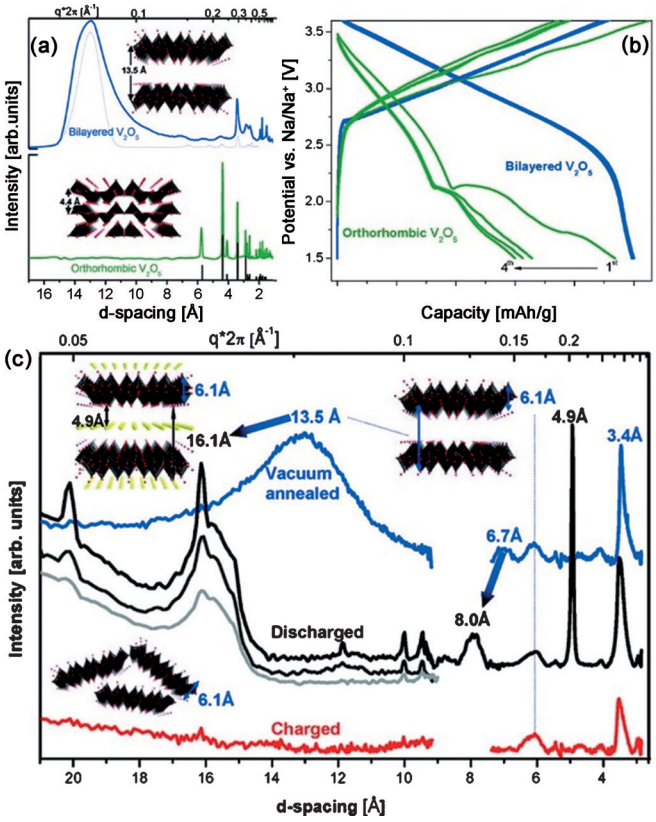

Figure 4. Synchrotron XRD and molecular simulations of electrodeposited vanadium oxide: a) bilayered and orthorhombic V_2O_5. b) First four dis/charge cycles of bilayered and orthorhombic V_2O_5 electrodes at 20 mA g^{-1} within the potential window of 3.8–1.5 V (vs. Na/Na$^+$). c) SAXS and WAXS spectra for as-deposited, discharged, and charged bilayered V_2O_5. Reprinted with permission from Tepavcevic et al., *ACS Nano* **2012**, *6*, 530–538. Copyright 2012 American Chemical Society.[79]

one another at regular intervals, in which the stacked bilayers are separated by large interlayer spacing of approximately 13.5 Å. However, it was observed that there was defective variation with the spacing between bilayers and that the atomic ordering of the overall structure was limited to the short-range scale. The bilayered V_2O_5 material was found to have a higher degree of local symmetry than its orthorhombic counterpart because of the decreased apical V–O bond length.

The bilayered V_2O_5 cathodes demonstrated a specific capacity of 250 mA h g^{-1} and were able to maintain 85% of their initial capacity after 350 cycles with the current density varying from 20 to 630 mA g^{-1}. The sodium intercalation performance of the orthorhombic material was significantly less at 150 mA h g^{-1} and rapidly decreased with cycling, despite the long-range order that could potentially enable unhindered diffusion. The mechanism of sodiation was also determined to be different, as revealed through the discharge potential profiles. Sodium-ion incorporation into the bilayered structure shows solid-state solution intercalation with no apparent phase transition, whereas the incorporation of Na^+ into the orthorhombic electrode is accompanied by two phase transitions. The ex situ characterization demonstrated that the deintercalation of bilayered V_2O_5 electrodes was accompanied by the loss of long-range order while short-range order was preserved. This phenomena was determined to be reversible and could be attributed to the electrostatic interaction between sodium ions and the terminal oxygen of the square-pyramidal VO_5 unit. Conversely, the orthorhombic V_2O_5 experienced deterioration and eventual loss of crystallinity after extended cycling. The results were reinforced in a imitative study.[78] These findings suggest the advantage of short-range-ordered structures deviating from the thermodynamic equilibrium for sodium-ion battery application.

Following a simple precipitation method, amorphous and crystalline V_2O_5 were prepared through various thermal treatments.[79] It was proposed that crystallographic Li^+ storage sites that are responsible for Li^+ trapping and irreversible phase transitions can be quenched by the incorporation of lattice disorder that can effectively discourage phase transitions. The amorphous material outperformed its crystalline counterpart with respect to reversible capacity, rate capability, and cycle performance. It was theorized that such discrepancy is due to vacant lattice sites and the enlarged accessible surface area that promote diffusion pathways throughout the amorphous V–O network. There was appreciable capacity loss for both crystalline and amorphous V_2O_5 in the first cycle (5 Li^+ ions lithiation, 2.6 Li^+ ions delithiation); however, the absence of peaks in the differential capacity versus voltage (d*Q*/d*V*) curves of the amorphous material revealed that this did not result from irreversible Li trapping, as was the case for crystalline V_2O_5. Further analysis determined that the irreversible capacity loss in the first cycle was due to a parasitic reaction with surface hydroxyl groups. This was effectively suppressed by removal of such hydroxyl groups by treatment with *n*-butyllithium.

The effects of crystallinity on vanadium pentoxide with respect to NIB performance were also recently investigated (Figure 5).[18] Amorphous and nanocrystalline V_2O_5 were prepared through a combination of sol–gel processes paired with electrochemical deposition and were investigated as a cathode for a sodium-ion battery. The amorphous V_2O_5 electrodes with short-range order and a more open framework demonstrated a discharge capacity of 241 mA h g^{-1} when examined as the positive electrode material for Na-ion battery applications, whereas its crystalline counterpart had only a capacity of 120 mA h g^{-1}. The significant difference between the crystalline and amorphous phases arises from the fast Faradaic reactions that occur in amorphous V_2O_5 stemming from a percolated diffusion network. Moreover, because diffusion now occurs through isotropic percolation and is not confined along a preferential pathway, the overall charging/discharging rates are much faster. The discrepancy in performance is primarily accredited to the low entropic energy associated with the ordering of intercalated atoms and a more open framework. The less structured and more open channels reduce the diffusion barrier for sodium ions to transition between sites, which leads to high rate capability and energy density.

Zhao et al. detailed the synergistic effect between crystal structure and intercalated ions both experimentally and theoretically. Most notably, they demonstrated that pre-intercalation of alkali-metal ions (Li, Na, K, Rb) in V–O can dramatically

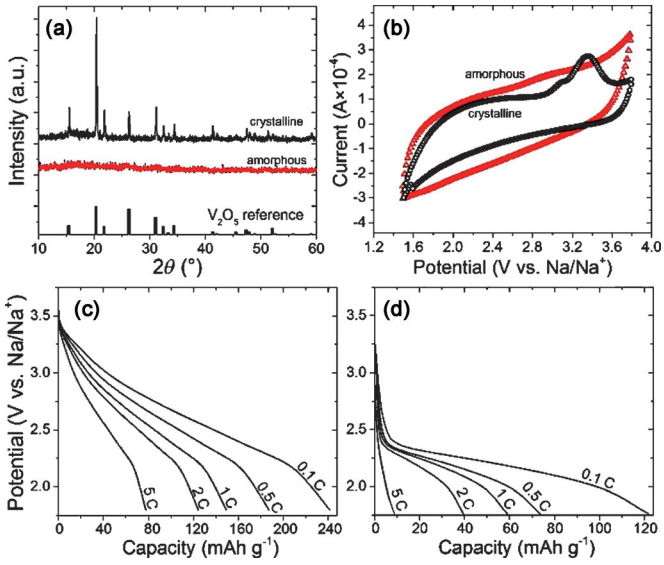

Figure 5. a) XRD spectra (with V_2O_5 reference) and CV plots (collected at 1.0 mV s^{-1}) for the amorphous (red) and crystalline (black) V_2O_5; and the rate capability of the c) amorphous and d) crystalline V_2O_5 when discharged at current densities ranging from 23.6 (0.1 C) to 1170 mA g^{-1} (5 C). Reproduced from Ref. [18] with permission from The Royal Chemistry Society.

improve the Li-ion cycling performance. However, this finding was not ubiquitous for all TMO systems as negligible or even negative changes in performance were observed for alkali-ion pre-intercalation in Co–O, Mn–O, and Fe-P-O. As resolved through DFT analysis, the diffusion barrier of pre-intercalated ions increases with cation size because of the interaction, and resulting distortion, with the terminal oxygen along the V–O diffusion layer. Although the interlayer diffusion of a large ion can be suppressed, this effectively hinders interlayer slippage and vertical collapse between layers, thus allowing Li ions to diffuse more freely. For pristine and pre-intercalated V_2O_5, the capacity retention after 100 cycles at 100 mA g^{-1} was 38 and 95%, respectively. The pre-intercalated compounds recorded lower initial capacity values, but they showed a diminished irreversible phase transition based on CV analysis.[80]

In a separate investigation, crystalline water was incorporated into the V_2O_5 lattice through the intercalation of water molecules. Although well known as a technique for bolstering the performance in a Li-ion setting, the new study was found to work for Na-ion battery applications as well.[81–83] The hydrated $V_2O_5{\cdot}nH_2O$, in which $n = 0.55$ as derived from TGA analysis, cathode displays an excellent sodium storage capability of 338 mA h g^{-1} at a current density of 50 mA g^{-1}, which is much higher than pristine, orthorhombic V_2O_5. More interestingly, CV characterization showed that a capacitive charge storage mechanism accounts for a significant proportion of the total observed capacity, and actually becomes more prevalent as the scan rate increases. Moreover, it was determined that the crystalline water is not totally exchanged during cycling based on ex situ XRD and FTIR analysis. These studies demonstrate that the optimized design of stable intercalation compounds could lead to substantial improvements in energy-storage applications.

6. Concluding Remarks

The aims of this focus review were to highlight how the positive effects of defect introduction in the development of optimized intercalation compounds could lead to substantial improvements for applications in energy storage. The defect types covered include, but are by no means limited to, cationic disordering, amorphization, doping, partial cation reduction, and manipulation of intrinsic defects. One of the main issues associated with defect introduction is the assurance of homogeneity; for example, the degree of amorphization can be difficult to reliably quantify/control. The summarized findings very clearly show the need to optimize the defect concentration, and the significance that balancing both the electronic and ionic transport can have on the achievement of high-rate-capability electrode materials. However, there is still significant work to be done to gain a solid fundamental understanding and, thus, control of the influences and impact of impurities on the processing, morphology, and properties of inorganic materials for application in energy conversion and storage.

Acknowledgements

Part of this work was financially supported by the National Science Foundation (NSF, CMMI-1030048) and a University of Washington TGIF grant. This material is based in part upon work supported by the State of Washington through the University of Washington Clean Energy Institute.

Keywords: defects · electrochemistry · energy storage · intercalation · materials science

[1] I. E. Agency, **2014**, 728.
[2] R. E. P. N. f. t. s. Century, **2014**.
[3] E. M. Erickson, C. Ghanty, D. Aurbach, *J. Phys. Chem. Lett.* **2014**, *5*, 3313.
[4] Y. Wang, B. Liu, Q. Li, S. Cartmell, S. Ferrara, Z. D. Deng, J. Xiao, *J. Power Sources* **2015**, *286*, 330.
[5] B. Nykvist, M. Nilsson, *Nature Clim. Change* **2015**, *5*, 329.
[6] M. Sathiya, A. M. Abakumov, D. Foix, G. Rousse, K. Ramesha, M. Saubanère, M. L. Doublet, H. Vezin, C. P. Laisa, A. S. Prakash, D. Gonbeau, G. VanTendeloo, J. M. Tarascon, *Nat. Mater.* **2015**, *14*, 230>.
[7] A. Sakti, J. J. Michalek, E. R. H. Fuchs, J. F. Whitacre, *J. Power Sources* **2015**, *273*, 966.
[8] Y. Liu, D. Liu, Q. Zhang, G. Cao, *J. Mater. Chem.* **2011**, *21*, 9969.
[9] Q. F. Zhang, E. Uchaker, S. L. Candelaria, G. Z. Cao, *Chem. Soc. Rev.* **2013**, *42*, 3127.
[10] J. Maier, *Nat. Mater.* **2005**, *4*, 805.
[11] J. B. Goodenough, Y. Kim, *Chem. Mater.* **2010**, *22*, 587.
[12] N. Yabuuchi, K. Kubota, M. Dahbi, S. Komaba, *Chem. Rev.* **2014**, *114*, 11636.
[13] M. D. Slater, D. Kim, E. Lee, C. S. Johnson, *Adv. Funct. Mater.* **2013**, *23*, 947.
[14] A. K. Padhi, K. S. Nanjundaswamy, J. B. Goodenough, *J. Electrochem. Soc.* **1997**, *144*, 1188.
[15] Z. Chen, J. Li, Z. Zhang, *J. Mater. Chem.* **2012**, *22*, 18968.
[16] B. C. Melot, J. M. Tarascon, *Acc. Chem. Res.* **2013**, *46*, 1226.
[17] J. Lee, A. Urban, X. Li, D. Su, G. Hautier, G. Ceder, *Science* **2014**, *343*, 519.
[18] E. Uchaker, Y. Z. Zheng, S. Li, S. L. Candelaria, S. Hu, G. Z. Cao, *J. Mater. Chem. A* **2014**, *2*, 18208.
[19] Y. Li, J. Yao, E. Uchaker, M. Zhang, J. Tian, X. Liu, G. Cao, *J. Phys. Chem. C* **2013**, *117*, 23507.

[20] D. Liu, Y. Liu, A. Pan, K. P. Nagle, G. T. Seidler, Y.-H. Jeong, G. Cao, *J. Phys. Chem. C* **2011**, *115*, 4959.
[21] K. J. Carroll, D. Qian, C. Fell, S. Calvin, G. M. Veith, M. Chi, L. Baggetto, Y. S. Meng, *Phys. Chem. Chem. Phys.* **2013**, *15*, 11128.
[22] C. R. Fell, D. Qian, K. J. Carroll, M. Chi, J. L. Jones, Y. S. Meng, *Chem. Mater.* **2013**, *25*, 1621.
[23] D. Qian, B. Xu, M. Chi, Y. S. Meng, *Phys. Chem. Chem. Phys.* **2014**, *16*, 14665.
[24] J. Song, D. W. Shin, Y. Lu, C. D. Amos, A. Manthiram, J. B. Goodenough, *Chem. Mater.* **2012**, *24*, 3101.
[25] P. V. Sushko, K. M. Rosso, J.-G. Zhang, J. Liu, M. L. Sushko, *Adv. Funct. Mater.* **2013**, *23*, 5530.
[26] M. Z. Bazant, *Acc. Chem. Res.* **2013**, *46*, 1144.
[27] G. K. Singh, G. Ceder, M. Z. Bazant, *Electrochim. Acta* **2008**, *53*, 7599.
[28] H. Y. Zhu, Y. Lan, X. P. Gao, S. P. Ringer, Z. F. Zheng, D. Y. Song, J. C. Zhao, *J. Am. Chem. Soc.* **2005**, *127*, 6730.
[29] X. H. Wang, J. G. Li, H. Kamiyama, M. Katada, N. Ohashi, Y. Moriyoshi, T. Ishigaki, *J. Am. Chem. Soc.* **2005**, *127*, 10982.
[30] K. Mizushima, P. C. Jones, P. J. Wiseman, J. B. Goodenough, *Mater. Res. Bull.* **1980**, *15*, 783.
[31] H. Duncan, B. Hai, M. Leskes, C. P. Grey, G. Chen, *Chem. Mater.* **2014**, *26*, 5374.
[32] M. R. Jo, Y.-I. Kim, Y. Kim, J. S. Chae, K. C. Roh, W.-S. Yoon, Y.-M. Kang, *ChemSusChem* **2014**, *7*, 2248.
[33] E. Lee, K. A. Persson, *Chem. Mater.* **2013**, *25*, 2885.
[34] D. W. Shin, C. A. Bridges, A. Huq, M. P. Paranthaman, A. Manthiram, *Chem. Mater.* **2012**, *24*, 3720.
[35] J. Xiao, X. Chen, P. V. Sushko, M. L. Sushko, L. Kovarik, J. Feng, Z. Deng, J. Zheng, G. L. Graff, Z. Nie, D. Choi, J. Liu, J.-G. Zhang, M. S. Whittingham, *Adv. Mater.* **2012**, *24*, 2109.
[36] E. Lee, K. A. Persson, *Energy Environ. Sci.* **2012**, *5*, 6047.
[37] L. Croguennec, M. R. Palacin, *J. Am. Chem. Soc.* **2015**, *137*, 3140.
[38] H.-T. Fang, M. Liu, D.-W. Wang, T. Sun, D.-S. Guan, F. Li, J. Zhou, T.-K. Sham, H.-M. Cheng, *Nanotechnology* **2009**, *20*, 225701.
[39] Y. Kim, Y. Park, A. Choi, N. S. Choi, J. Kim, J. Lee, J. H. Ryu, S. M. Oh, K. T. Lee, *Adv. Mater.* **2013**, *25*, 3045.
[40] G. Venkatesh, V. Pralong, O. I. Lebedev, V. Caignaert, P. Bazin, B. Raveau, *Electrochem. Commun.* **2014**, *40*, 100.
[41] H. Xiong, M. D. Slater, M. Balasubramanian, C. S. Johnson, T. Rajh, *J. Phys. Chem. Lett.* **2011**, *2*, 2560.
[42] C. M. Julien, *Mater. Sci. Eng. R* **2003**, *40*, 47.
[43] J. Kim, A. Manthiram, *Nature* **1997**, *390*, 265.
[44] T. R. Paudel, A. Zakutayev, S. Lany, M. d'Avezac, A. Zunger, *Adv. Funct. Mater.* **2011**, *21*, 4493.
[45] J. A. Kilner, R. J. Brook, *Solid State Ionics* **1982**, *6*, 237.
[46] J.-Y. Luo, L.-J. Chen, Y.-J. Zhao, P. He, Y.-Y. Xia, *J. Power Sources* **2009**, *194*, 1075.
[47] S.-Y. Chung, J. T. Bloking, Y.-M. Chiang, *Nat. Mater.* **2002**, *1*, 123.
[48] L. Dahéron, H. Martinez, R. Dedryvère, I. Baraille, M. Ménétrier, C. Denage, C. Delmas, D. Gonbeau, *J. Phys. Chem. C* **2009**, *113*, 5843.
[49] M. Murakami, Y. Noda, Y. Koyama, K. Takegoshi, H. Arai, Y. Uchimoto, Z. Ogumi, *J. Phys. Chem. C* **2014**, *118*, 15375.
[50] S. Y. Hong, Y. Kim, Y. Park, A. Choi, N.-S. Choi, K. T. Lee, *Energy Environ. Sci.* **2013**, *6*, 2067.
[51] D. Datta, J. Li, V. B. Shenoy, *ACS Appl. Mater. Interfaces* **2014**, *6*, 1788.
[52] J. M. Clark, P. Barpanda, A. Yamada, M. S. Islam, *J. Mater. Chem. A* **2014**, *2*, 11807.
[53] D. R. Rolison, B. Dunn, *J. Mater. Chem.* **2001**, *11*, 963.
[54] B. Guo, X. Wang, P. F. Fulvio, M. Chi, S. M. Mahurin, X.-G. Sun, S. Dai, *Adv. Mater.* **2011**, *23*, 4661.
[55] A. L. M. Reddy, A. Srivastava, S. R. Gowda, H. Gullapalli, M. Dubey, P. M. Ajayan, *ACS Nano* **2010**, *4*, 6337.
[56] D. Y. Pan, S. Wang, B. Zhao, M. H. Wu, H. J. Zhang, Y. Wang, Z. Jiao, *Chem. Mater.* **2009**, *21*, 3136.
[57] L.-J. Zhou, Z. F. Hou, L.-M. Wu, Y.-F. Zhang, *J. Phys. Chem. C* **2014**, *118*, 28055.
[58] Y. Cao, L. Xiao, M. L. Sushko, W. Wang, B. Schwenzer, J. Xiao, Z. Nie, L. V. Saraf, Z. Yang, J. Liu, *Nano Lett.* **2012**, *12*, 3783.
[59] D. A. Stevens, J. R. Dahn, *J. Electrochem. Soc.* **2001**, *148*, A803.
[60] D. Datta, J. Li, N. Koratkar, V. B. Shenoy, *Carbon* **2014**, *80*, 305.
[61] J. C. Pramudita, D. Pontiroli, G. Magnani, M. Gaboardi, M. Riccò, C. Milanese, H. E. A. Brand, N. Sharma, *ChemElectroChem* **2015**, *2*, 600.
[62] R. Mukherjee, A. V. Thomas, D. Datta, E. Singh, J. Li, O. Eksik, V. B. Shenoy, N. Koratkar, *Nat. Commun.* **2014**, *5*, 3710.
[63] Y. Wen, K. He, Y. Zhu, F. Han, Y. Xu, I. Matsuda, Y. Ishii, J. Cumings, C. Wang, *Nat. Commun.* **2014**, *5*, 4033.
[64] P. C. Tsai, S. C. Chung, S. K. Lin, and A. Yamada, *J. Mater. Chem. A* **2015**, *3*, 9763.
[65] M. Saiful Islam, D. J. Driscoll, C. A. J. Fisher, P. R. Slater, *Chem. Mater.* **2005**, *17*, 5085.
[66] K. Hoang, M. D. Johannes, *J. Mater. Chem. A* **2014**, *2*, 5224.
[67] H. Duan, J. Li, H. Du, S. W. Chiang, C. Xu, W. Duan, F. Kang, *J. Phys. Chem. C* **2015**, *119*, 5238.
[68] A. Magnéli, B. Blomberghansson, L. Kihlborg, G. Sundkvist, *Acta Chem. Scand.* **1955**, *9*, 1382.
[69] J.-Y. Shin, J. H. Joo, D. Samuelis, J. Maier, *Chem. Mater.* **2012**, *24*, 543.
[70] J.-Y. Shin, D. Samuelis, J. Maier, *Solid State Ionics* **2012**, *225*, 590.
[71] D. Liu, Y. Zhang, P. Xiao, B. B. Garcia, Q. Zhang, X. Zhou, Y.-H. Jeong, G. Cao, *Electrochim. Acta* **2009**, *54*, 6816.
[72] H. Furukawa, M. Hibino, I. Honma, *J. Electrochem. Soc.* **2004**, *151*, A527.
[73] M. Hibino, K. Abe, M. Mochizuki, M. Miyayama, *J. Power Sources* **2004**, *126*, 139.
[74] A. F. Gross, C. C. Ahn, S. L. Van Atta, P. Liu, J. J. Vajo, *Nanotechnology* **2009**, *20*, 204005.
[75] K. E. Swider-Lyons, C. T. Love, D. R. Rolison, *Solid State Ionics* **2002**, *152*, 99.
[76] K. Takahashi, S. J. Limmer, Y. Wang, G. Cao, *J. Phys. Chem. B* **2004**, *108*, 9795.
[77] S. Tepavcevic, H. Xiong, V. R. Stamenkovic, X. Zuo, M. Balasubramanian, V. B. Prakapenka, C. S. Johnson, T. Rajh, *ACS Nano* **2012**, *6*, 530.
[78] H.-Y. Li, C.-H. Yang, C.-M. Tseng, S.-W. Lee, C.-C. Yang, T.-Y. Wu, J.-K. Chang, *J. Power Sources* **2015**, *285*, 418.
[79] O. B. Chae, J. Kim, I. Park, H. Jeong, J. H. Ku, J. H. Ryu, K. Kang, S. M. Oh, *Chem. Mater.* **2014**, *26*, 5874.
[80] Y. Zhao, C. Han, J. Yang, J. Su, X. Xu, S. Li, L. Xu, R. Fang, H. Jiang, X. Zou, B. Song, L. Mai, Q. Zhang, *Nano Lett.* **2015**, *15*, 2180.
[81] Q. Wei, J. Liu, W. Feng, J. Sheng, X. Tian, L. He, Q. Anb, L. Mai, *J. Mater. Chem. A* **2015**, *3*, 8070.
[82] Y. Wang, K. Takahashi, K. H. Lee, G. Z. Cao, *Adv. Funct. Mater.* **2006**, *16*, 1133.
[83] Y. Wang, H. Shang, T. Chou, G. Cao, *J. Phys. Chem. B* **2005**, *109*, 11361.

Manuscript received: April 17, 2015
Accepted article published: May 22, 2015
Final article published: June 23, 2015